World Academy of Science, Engineering and Technology
International Journal of Mathematical and Computational Sciences
Vol:7, No:6, 2013

3-D Reconstruction of Objects Using Digital Fringe Projection: Survey and Experimental Study

R. Talebi, A. Abdel-Dayem, and J. Johnson

***Abstract*—**Three-dimensional reconstruction of small objects has been one of the most challenging problems over the last decade. Computer graphics researchers and photography professionals have been working on improving 3D reconstruction algorithms to fit the high demands of various real life applications. Medical sciences, animation industry, virtual reality, pattern recognition, tourism industry, and reverse engineering are common fields where 3D reconstruction of objects plays a vital role. Both lack of accuracy and high computational cost are the major challenges facing successful 3D reconstruction. Fringe projection has emerged as a promising 3D reconstruction direction that combines low computational cost to both high precision and high resolution. It employs digital projection, structured light systems and phase analysis on fringed pictures. Research studies have shown that the system has acceptable performance, and moreover it is insensitive to ambient light.

This paper presents an overview of fringe projection approaches. It also presents an experimental study and implementation of a simple fringe projection system. We tested our system using two objects with different materials and levels of details. Experimental results have shown that, while our system is simple, it produces acceptable results.

***Keywords*—**Digital fringe projection, 3D reconstruction, phase unwrapping, phase shifting.

I. Introduction

THREE-dimensional reconstruction of both actual objects and the surrounding environment has always been one of the primary goals of short-range photogrammetric. This is due to the need of measuring and visualizing real world in various applications. As an example of such applications, virtual world like reality is currently one of the most active research topics. Three-dimensional reconstruction of the real world is the stepping-stone toward the construction of a model for each object (virtual world).Virtual world can be used in animations, cinema, and computer games industry. Fringe projection shape measurement is one of the most widely used techniques in practical applications of three-dimensional (3D) shape measurements (e.g. object detection, digital model generation, object replication, reverse engineering, rapid prototyping, product inspection, and quality control). A structured light system is similar to a stereo technique as it only uses two devices for 3D shape measurement. However, fringe projection replaces one camera of a stereo system with a projector to project structured patterns, which are encoded through certain codification strategies. Then, the captured structured patterns are decoded. If the code-words (used to encode the structured pattern) are unique, the correspondence between the projector sensor and the camera sensor is uniquely identified, and 3D information can be calculated through triangulation. Generally, structured light systems use binary patterns, where only 0 and 1 s are used for codification. Binary patterns are easier to encode and decode, resulting in a considerable performance gain for the overall system. Moreover, it is robust to noise.

Recent progress in digital imaging has greatly boosted three-dimensional measurements of objects. Please, note that conventional coordinate measuring machines are incapable to cope with real application, as point-to-point measurements are extremely time consuming. Three-dimensional measurement techniques are broadly classified into two categories; contact and non-contact approaches, refer to Fig. 1. We will limit our discussion to fringe projection as an effective non-contact approach.

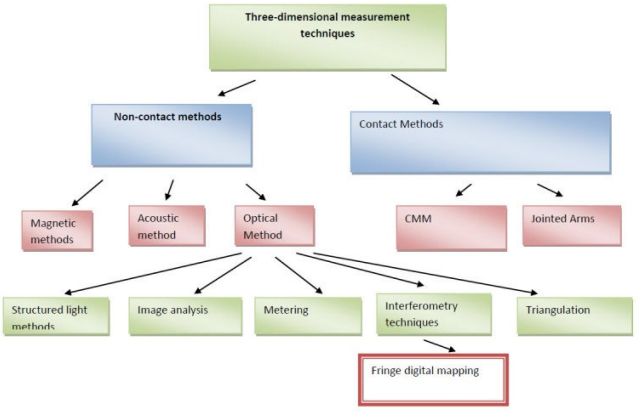

Fig. 1 Three dimensional reconstructed systems

Figs. 2 and 3 highlight the arrangements and the major stages of a fringe projection approach, which starts by projecting a sinusoidal pattern over the surface of the object, using a projector. Then, a digital camera is used to capture the pattern that has been assorted (phase modulated) by the

R. Talebi is an M.Sc. student in the Department of Mathematics and Computer Science, at Laurentian University, Sudbury, Ontario, Canada (e-mail: Rx_Talebi@laurentian.ca).

A. Abdel-Dayem is an Assistant professor at the Department of Mathematics and Computer Science, at Laurentian University, Sudbury, Ontario, Canada (e-mail: aabdeldayem@cs.laurentian.ca).

J. Johnson is an Associate professor at the Department of Mathematics and Computer Science, at Laurentian University, Sudbury, Ontario, Canada (e-mail: jjohnson@cs.laurentian.ca).

topography of the object surface. Finally, the captured pattern is analyzed to extract relevant topographical information about the object. Note that, phase modulation analysis uses the *arctan* function, which yields values in the range $[-\pi,+\pi]$. However, true phase values may extend over 2π range, resulting in discontinuities in the recovered phase. Phase unwrapping aims at adding integral multiples of 2π at each pixel to remove such discontinuity. Then, three-dimensional coordination of each pixel is computed by converting the unwrapped phase to depth (height).

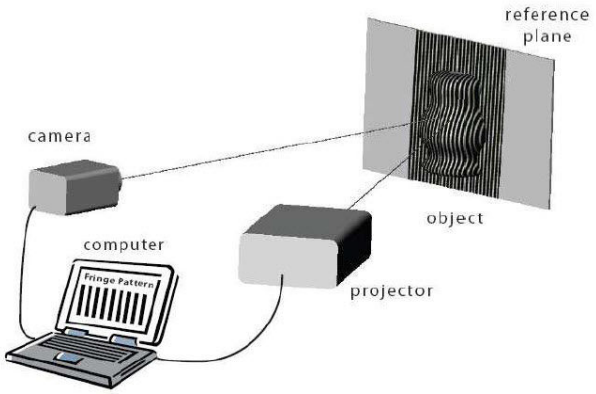

Fig. 2 Fringe projection arrangement

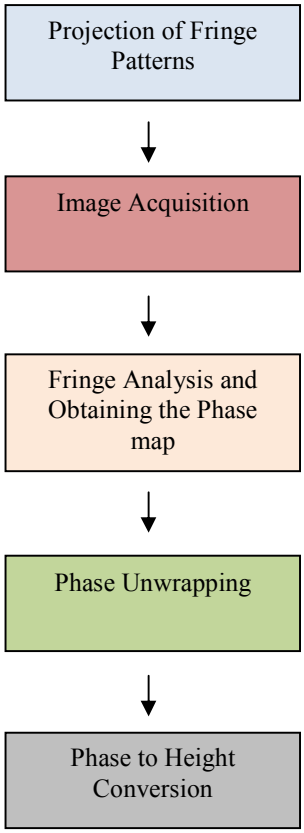

Fig. 3 Fringe projection phases

The paper is organized as follows. Section II highlights previous research studies for fringe analysis. Then, Section III and Section IV present the experimental set up and results, respectively. Finally, Section V offers concluding remarks and suggestions for future work.

II. Prior and Related Work

Fringe digital mapping was first proposed by Rowe *et al.* [1] in 1967. Since then, it has been used in various applications in both research and industry. While, fringe projection approach employs four stages (refer to Fig. 3), we will focus our discussion on the fringe analysis and phase detection stage due to its contribution toward the success of the overall system.

Phase detection has been one of the most active research areas over the last decade. It can be broadly classified into two main categories:

- Time-based analysis
- Frequency-based analysis

While the success of time-based analysis approaches highly depends on the appropriate selection of the number of phase transitions, frequency-based approaches depend on the carrier frequency.

Common phase detection approaches found in literature were based on either Fourier transform [2]-[9], interpolated Fourier transform [10], continuous wavelet transform [11]-[13], two dimensional continues wavelet transform, discrete consign transform, neural network, phase locked loop, spatial phase detection, or phase transition [14].

Quan *et al.* [15] proposed the phase transition approach for small object measurement. In 2001, Berryman *et al.* [16] compared three different approaches (Fourier transform, phase transition, and spatial phase detection) on the reconstruction of a sphere using simulated data. Their experiments showed that in low noise conditions, phase transition produces the best results. With more than 10% noise, using Fourier transform would be a good choice. However, on high noise levels spatial phase detection showed superior results.

Suutton *et al.* [17] proposed a phase detection scheme based on the use of Hilbert transform with Laplacian pyramid. The proposed scheme produces high precision level.

Gdeisat *et al.* [18] used two-dimensional continuous wavelet transform to eliminate the low component's frequency of the fringe. Then, Fourier transform was employed for phase detection. This method offers acceptable results; taking into consideration that it uses only one fringe.

Su *et al.* [19] used two-dimensional Fourier transform for phase detection and modeling. By employing a time delay integration high-speed camera and a turntable, a 360-degree image of an object was recorded. Then, a complete three-dimensional model was produced. Fig. 4 shows a sample of a 360 degree recorded image, while Fig. 5 shows a three-dimensional model of a statue produced by [19].

(a) (b)

Fig. 4 (a) The detected phase, (b) After applying the two-dimensional Fourier transform and phase unwrapping [19]

Fig. 5 Three-dimensional reconstruction [19]

Tangy *et al*. [20] used a neural network based approach to extract the phase from the fringed image. Fourier transform is employed without any filtration. As a result, high frequency details were preserved.

Zhang *et al*. [21] used a Digital Micro-mirror Device (DMD) and a projector with 40 frames per second to reconstruct a three-dimensional model using the phase transition method. They employed three separate fringe patterns in the red, green and blue channels.

The following subsections present quick overview of fringe pattern analysis, phase unwrapping, and phase to height conversion, respectively.

A. Fringe Pattern Analysis Techniques

1. Fringe Pattern Analysis Using Wavelet Transform

During the last decade, Wavelet transform has become a promising tool in areas; like phase demodulation of fringe patterns, and has sustained notable progressions with respect to this application. The advantage of using wavelet transform on non-stationary signals over stationary signals has been proved. A stationary signal (Fig. 6) is a signal whose frequency contents do not change in time, whereas a non-stationary signal (Fig. 7) is a signal whose frequency contents change in time or position [22].

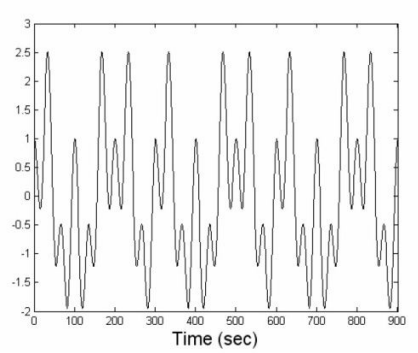

Fig. 6 Stationary signal example [22]

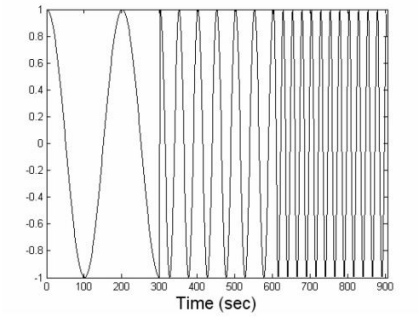

Fig. 7 A non-stationary signal example [22]

Fringe patterns represent non-stationary spatial signals. The following figure represents a real non-stationary signal, which is an actual representation of one row of a fringe pattern:

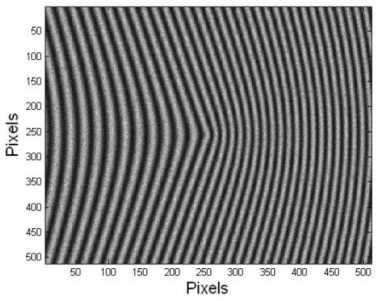

Fig. 8 Fringe pattern example [23]

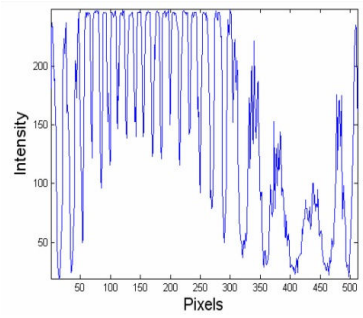

Fig. 9 A non-stationary signal of one row of the represented fringe pattern [23]

Various techniques have been proposed based on one-dimensional continuous wavelet transform (1D-CWT). These techniques can be broadly classified into two main categories:

- Phase estimation
- Frequency estimation

In phase estimation techniques, the image is processed row-by-row using continuous wavelet transform (1D-CWT). The result is a two dimensional array of complex coefficients, which can be divided into magnitude and phase. Then, ridges are extracted using one of the common available ridge extraction algorithms [6]-[8]. Finally, the wrapped phase of the extracted ridge is unwrapped.

The following figure represents an illustration of phase estimation method to extract the phase from the simulated fringe pattern that was originally shown in Fig. 8. Fig. 10 (a) shows the absolute value array that results from the analysis of one row of fringe pattern (1D-CWT). Ridges have been extracted using the maximum method, and they are represented by a solid line. Fig. 10 (b) represents the phase value array for the previous row. The solid line shows the wrapped phase corresponding to the row under consideration. Fig. 10 (c) shows the wrapped phase map, while Fig. 10 (a) represents the 3D representation of the unwrapped phase (after subtracting the carrier).

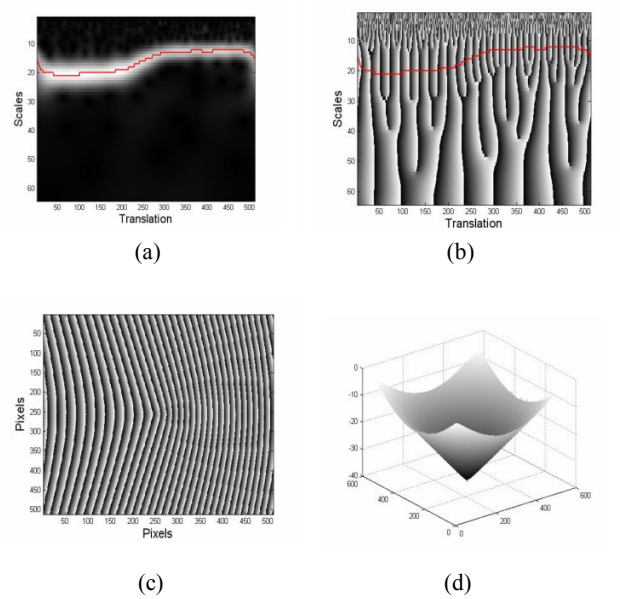

Fig. 10 (a) Absolute value array of a row (b) Phase value array (c) Unwrapped phase (d) 3D view of the unwrapped phase [23]

In frequency estimation techniques, ridge values are calculated using same approaches as in phase estimation techniques. Then, scale values can be calculated at the positions where these ridges are located. Instantaneous frequencies are estimated from those calculated scale values. Finally, by integration of these estimated frequency values, the unwrapped phase can be extracted directly without the need of phase unwrapping process.

Fig. 11 shows a 3D output using frequency estimation method for the same input fringe shown in Fig. 8.

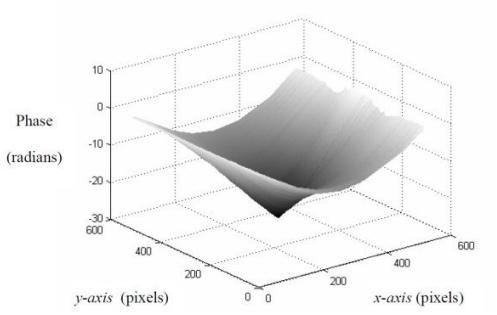

Fig. 11 3D phase distribution using the frequency estimation method [23]

2. Fringe Pattern Analysis Using Fourier Transform

Fourier Transform was first used for fringe analysis and phase extraction by Takeda *et al*. in 1982 [24]. Later on, various improvements were proposed [25]-[28].While phase transition approaches use three images to extract the modulated phase; Fourier transform-based approaches use only one image. In sequel, a brief description of phase extraction using Fourier transform is presented.

The intensity profile of a fringe pattern is given by:

$$\boldsymbol{g(x,y) = a(x,y) + \frac{1}{2} b(x,y) \times [e^{i(2\pi f_0 x + \varphi(x,y))} + e^{-i(2\pi f_0 x + \varphi(x,y))}]} \quad (1)$$

where, $a(x,y)$ is the background intensity, $b(x,y)$is the amplitude modulation of fringes, $f_0$is the spatial carrier frequency, $\varphi(x,y)$is the phase modulation of fringes (the required phase distribution).

Takeda *et al*. [24] represented (1) as:

$$g(x,y) = a(x,y) + c(x,y).e^{i2\pi f_0 x} + c^*(x,y).e^{-i2\pi f_0 x} \quad (2)$$

where, $c(x,y) = \frac{1}{2} b(x,y).e^{i\varphi(x,y)}$, and$c^*(x,y) = \frac{1}{2} b(x,y).e^{-i\varphi(x,y)}$

Taking the one-dimensional Fourier Transform on the x direction:

$$G(f_x,y) = A(f_x,y) + C(f_x - f_0,y) + C^*(f_x + f_0,y) \quad (3)$$

where, $A(f_x,y)$is the spectrum of the background intensity (illumination of the measured scene), $C(f_x - f_0,y)$, and $C^*(f_x + f_0,y)$are the spectra of the deformed fringes. Note that, $C$and C^* are symmetrical. Thus, it is sufficient to extract either one. $C(f_x - f_0,y)$ can be extracted by using a filtering process, as shown in Fig. 12. Then, inverse Fourier transform is used to transform $C(f_x - f_0,y)$ back to the spatial domain $c(x,y)$. Finally, the phase information can be calculated as:

$$\varphi(x,y) = tan^{-1}\left(\frac{Im[c(x,y)]}{Re[c(x,y)]}\right) \quad (4)$$

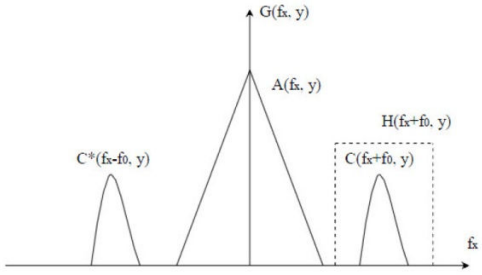

Fig. 12 Filtering the spectrum of the deformed fringes [28]

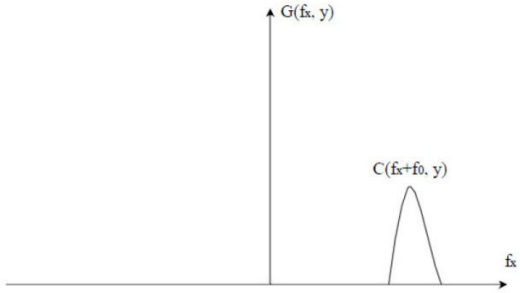

Fig. 13 The extracted spectrum of the deformed fringes [28]

As an illustrative example, Fig. 14 shows a cylindrical shape object with fringe pattern projected on it:

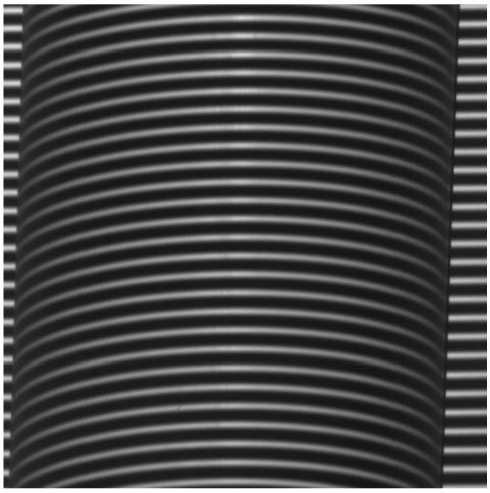

Fig. 14 Example of modulated fringe pattern on a cylindrical shape object [28]

Fig. 15 shows the frequency spectrum of the image shown in Fig. 14. The high peak in the center represents the background information (low frequency components), whereas, the other two symmetrical peaks represent the spectra of the deformed fringes. Using an appropriate filter window, the spectra of the deformed fringes can be extracted. Then, inverse Fourier transform is used to return back to the spatial domain, where the phase information can be extracted as shown in (4). Fig. 16 shows the extracted phase information before and after unwrapping. Fig. 17 shows the unwrapped phase in a 3D environment:

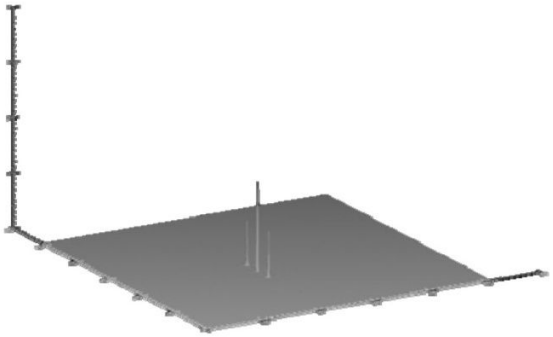

Fig. 1 Frequency spectrum obtained by applying a 2D Fourier transform to the input image from Fig. [28]

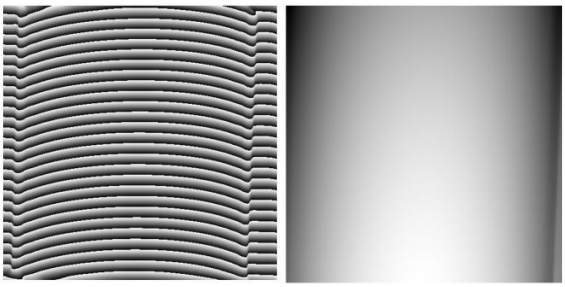

(a) (b)

Fig. 2 (a) Unwrapped phase (b) wrapped phase [28]

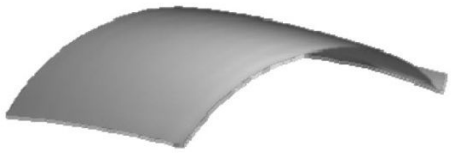

Fig. 37 3D plot of the phase image [28]

The previous example illustrates the advantages of using Fourier transform in fringe analysis, where a single image is needed. This feature is particularly useful when measuring mobile objects and/or real time measurements. Moreover, it is stable on measuring areas and objects that are relatively flat and without discontinuities (e.g. in medical fields for measuring organ surfaces). However, the output quality highly depends on the accuracy of both the filtering stage in the frequency domain and the phase unwrapping stage, as well. Moreover, noise may have negative impact on the final output.

B. Fringe Pattern Analysis Using Phase Shifting

The image of a projected pattern can be written as:

$$g(x,y) = a(x,y) + b(x,y)\cos(2\pi f_0 x + \varphi(x,y)) \quad (5)$$

where, $a(x,y)$ is the background intensity, $b(x,y)$is the amplitude modulation of fringes, $f_0$is the spatial carrier frequency, $\varphi(x,y)$is the phase modulation of fringes (the required phase distribution). Equation (5) contains three unknowns; $a(x,y)$, $b(x,y)$, and $\varphi(x,y)$. As a result, three

independent equations are needed to eliminate $a(x,y)$ and $b(x,y)$. This goal can be achieved by using three identical fringe patters shifted by known amounts (2π/3 radians). This leads to the following three equations:

$$g_1(x,y) = a(x,y) + b(x,y)\cos(2\pi f_0 x + \varphi(x,y) - \tfrac{2}{3}\pi) \quad (6)$$

$$g_2(x,y) = a(x,y) + b(x,y)\cos(2\pi f_0 x + \varphi(x,y)) \quad (7)$$

$$g_3(x,y) = a(x,y) + b(x,y)\cos(2\pi f_0 x + \varphi(x,y) + \tfrac{2}{3}\pi) \quad (8)$$

Solving the above three equations, the phase $\varphi(x,y)$can be obtained as:

$$\varphi(x,y) = tan^{-1}\frac{\sqrt{3}(g_1 - g_3)}{2g_2 - g_1 - g_3} \quad (9)$$

It is evident that, phase shifting approach is less prone to both noise and filtration distortions, compared to Fourier transform approaches. However, three fringe images are required to extract phase information.

1. Phase Unwrapping

Fringe analysis stage computes the phase $\varphi(x,y)$ using the *arctangent* function which produces values in the range between –π and +π. The phase map computed by this step is called wrapped phase map. It suffers from discontinuities of values of 2π. Thus, it is necessary to identify multiples of 2π to be added to the phase value at each pixel to yield continuous phase values. This process is called phase unwrapping.

Normal phase unwrapping is carried out by matching the phase at neighboring pixels and adding or subtracting 2π to bring the relative phase between two pixels into the range of –π to +π. Thus, phase unwrapping is a trivial task if the wrapped phase map is ideal. However, in real measurements various factors (e.g. the presence of shadows, low fringe modulations, non-uniform reflectivity of the object surface, fringe discontinuities, noise) influence phase unwrapping. Various research studies have been proposed to tackle these challenges, however they are outside the scope of this paper.

2. Phase to Height Conversion

After phase unwrapping, height information of the measured object can be extracted. There are two common approaches to calculate depth information from unwrapped phase map: relative coordinate calculation and absolute coordinate calculation. Absolute coordinate calculation approach is based on triangulation to estimate the absolute coordinate of every pixel in the world coordinate system. This approach requires precise knowledge about intrinsic and extrinsic parameters of both camera and projector. Thus, a system calibration step is essential. On the other hand, the relative approach calculates the depth of each pixel using a reference plane. It does not require a calibration process. Moreover, the relative depth calculation approach is computationally less expensive compared to the absolute approach. Fig. 18 shows a schematic diagram that illustrates the relative depth calculation approach. Points P and I are the perspective centers of the DLP projector and the CCD camera, respectively. The optical axes of the projector and the camera coincide at point O. After the system has been set up, a flat reference plane is measured first whose phase map is used as a reference for subsequent measurements. Then, the height of the object surface is measured relative to this reference plane [21].

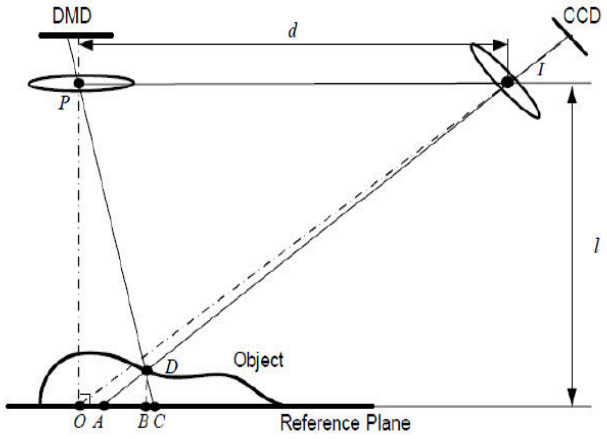

Fig. 48 Schematic diagram of phase-to-height conversion using the relative depth calculation approach

From the projector point of view, point *D* on the object surface has identical phase value as point *C* on the reference plane, i.e. $\varphi_D = \varphi_C$. On the other hand, from the CCD camera point of view, point *D* on the object surface and point *A* on the reference plane are imaged on the same pixel. By subtracting the reference phase map from the object phase map, we obtain the phase difference at this specific pixel:

$$\varphi_{AD} = \varphi_{AC} = \varphi_A - \varphi_C \quad (10)$$

Assume that points *P* and *I* are planned to be on the equivalent plane with a distance *l* to the reference plane and have a distance *d* between them, and the reference plane is parallel to the device. Hence, the triangles *PID* and *CAD* in Fig. 18 are similar. Therefore:

$$\frac{d}{\overline{AC}} = \frac{l - \overline{DB}}{\overline{DB}} = \frac{l}{\overline{DB}} - 1 \quad (11)$$

where, *d* is the distance between the camera and the projector. Since *d* is much larger than *AC* for real measurement, this equation can be simplified as:

$$h(x,y) = \overline{DB} \cong \frac{1}{d}\overline{AC} = \frac{1}{d}\frac{\varphi_{AC}}{2\pi f} = K.\varphi_{AC} \quad (12)$$

where, *f* is the frequency of the projected fringes in the reference plane, *K* is a constant coefficient, and φ_{AC} is the phase containing the height information.

III. Experimental Setup

To conduct the experiments presented in this paper, we built a projection system with the configuration shown in Fig. 2. Our system is composed of an Optoma EP719 digital light processing unit (DLP), a PC with Intel Core i3 processor, and a Samsung NX10 camera. The DLP has the following technical specifications: 2000 ANSI lumens, 2500:1 contrast ratio, 4:3 aspect ratio, and a 1024x768 resolution. The DLP chip is a 2x rotation speed color wheel, and computer resolution is up to SXGA + (1400x1050). The camera has a resolution of 14.6 mega pixels and a kit lens of 18-55 mm. A tripod was used to fix the camera during the experiments. Two objects were used in our experiments. The first one is a chalky white sculpture of a woman without any sudden change in depth in its topography. The second object is a human skull with significant changes in depth in the eye area. We used the phase shifting approach (as explained in Section II.B) during the fringe pattern analysis phase. In each experiment, three fringe patterns, with phase shifts of $-2\pi/3$,0, and $2\pi/3$, were used. The experiments were repeated for various carrier frequencies. The results are presented in the next section.

IV. Experimental Results

A. Creating the Fringe Patterns

We used Matlab to create the fringe patterns and to process the images. Fig. 19 and Fig. 20 present samples of the fringe patterns used in our experimentations.

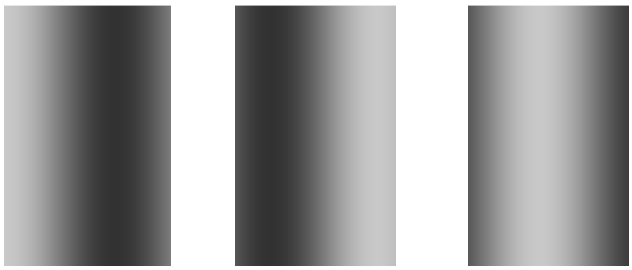

(a) (b) (c)

Fig. 5 Fringe patterns with minimum gray value of 50 and maximum gray value of 200, maximum projector resolution 1024 -768, a wavelength of 1024, and fringe transitions of (a) $-2\pi/3$, (b) $2\pi/3$, (c) zero

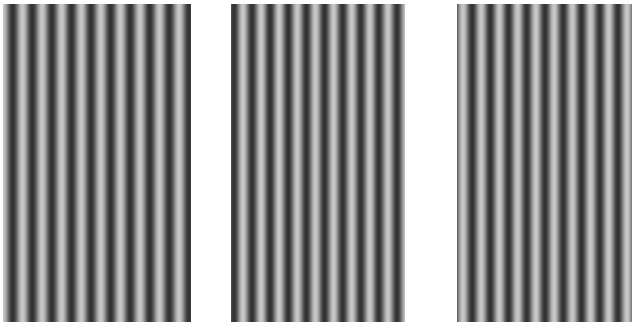

(a) (b) (c)

Fig. 20 Fringe patterns with minimum gray value of 50 and maximum gray value of 200, maximum projector resolution 1024 -768, a wavelength of 80, and fringe transitions of: (a) $-2\pi/3$, (b) $2\pi/3$, (c) zero

Note that, using fringe patterns with smaller wavelengths produce higher precision; however, it takes more time during the phase unwrapping stage.

B. Projecting the Patterns on the Object

Fringe patterns described in the previous subsection were projected on the two objects (human skull and woman sculpture), explained in Section III. These objects have different sizes, material, and level of details. We plan to extend our experiments on future to include more objects.

Fig. 21 and Fig. 22 show fringe patterns with wavelengths of 1024 and 10, respectively, projected on the same skull with phase transitions of $-2\pi/3$, $2\pi/3$, and zero, respectively.

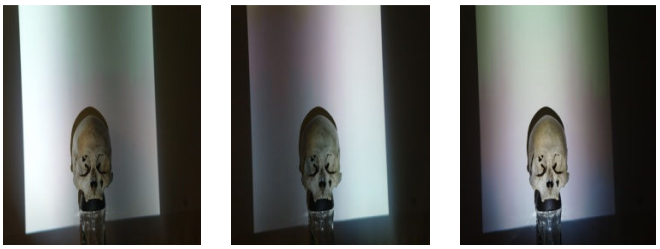

(a) (b) (c)

Fig. 21 Fringe patterns with wavelength of 1024 projected on the skull with transition of:(a)-$2\pi/3$, (b)$2\pi/3$, (c) zero

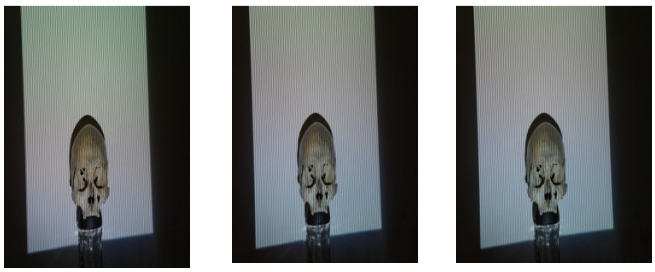

(a) (b) (c)

Fig. 6 Fringe patterns with wavelength of 10 projected on the skull with transition of:(a) $-2\pi/3$, (b) $2\pi/3$, (c) zero

Fig. 23 and Fig. 24 show fringe patterns with wavelengths of 1024 and 80, respectively, projected on the woman sculpture with phase transitions of -2π/3, 2π/3, and zero, respectively.

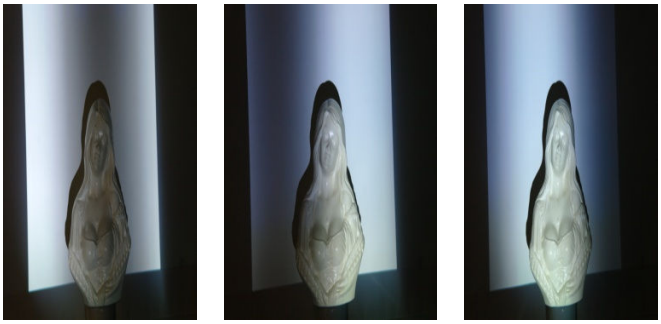

(a) (b) (c)

Fig. 7 Fringe patterns with wavelength of 1024 projected on the woman sculpture with phase transitions of (a) -2π/3, (b) 2π/3, (c) zero

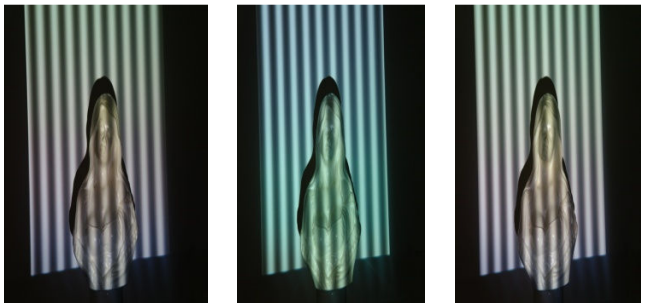

(a) (b) (c)

Fig. 24 Fringe patterns with wavelength of 80 projected on the woman sculpture with phase transition of (a) -2π/3, (b) 2π/3, (c) zero

Fig. 25 illustrates fringe analysis of the woman sculpture using a pattern with wavelength of 1024.

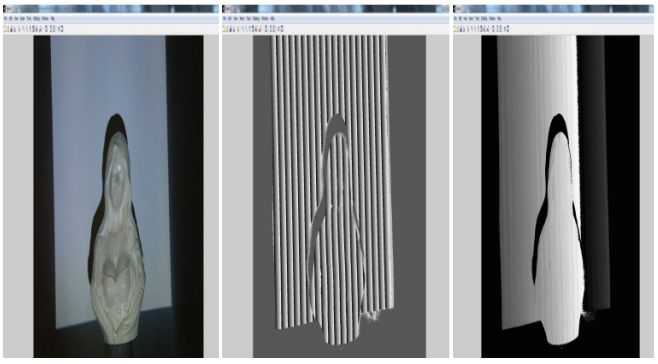

(a) (b) (c)

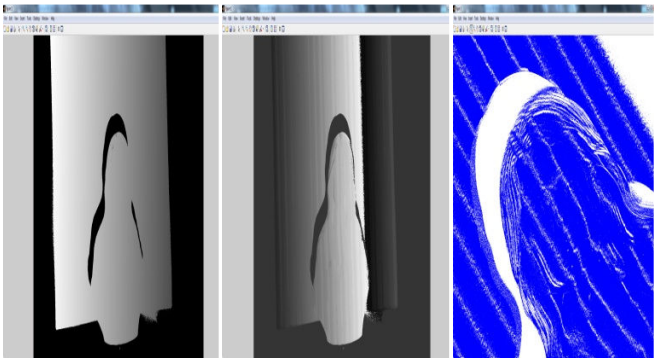

(d) (e) (f)

Fig. 85 Using fringe pattern with wavelength of 1024, (a) The original image without the fringe patterns, (b) the woman sculpture phase, (c) unwrapped phase, (d) plane source phase, (e) depth phase, (f) the 3Dcloud point output using plot3 command in Matlab

As Fig. 25 shows, the reconstructed 3D model does not produce high precision level and details, especially on lower level parts of the sculpture. However, it produces better precision on the higher coordinates of the sculpture, like the woman's hair in Fig. 26 (f).This is a direct result of using a fringe pattern wavelength that is not narrow enough to cover the details in low coordinates of the sculpture. Consequently, we decided to employ an extra fringe pattern with wavelength of 10 (shifted by -2π/3, 2π/3, and zero, respectively) to capture more details. Using the six captured images (three for each wavelength), better output was produced in this test case, as shown in Fig. 26.

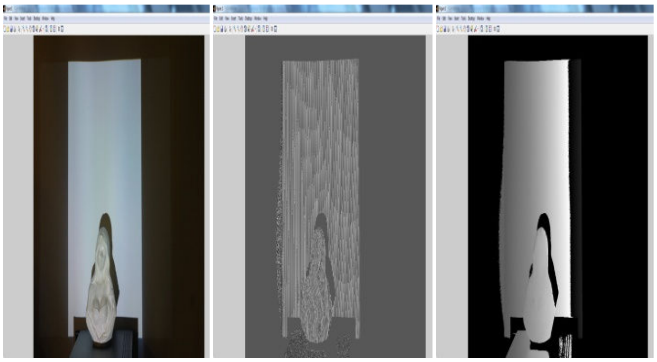

(a) (b) (c)

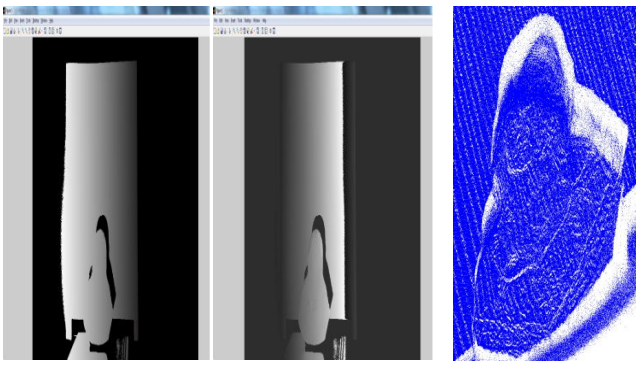

(d) (e) (f)

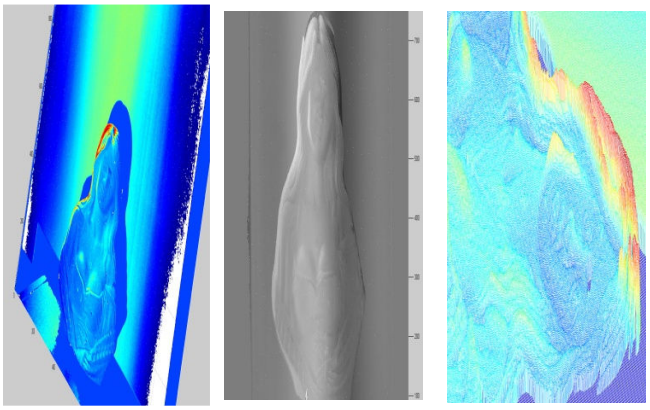

(g) (h) (i)

Fig. 9 Using fringe pattern with wavelength of 10, (a) The original image without the fringe patterns, (b) the woman sculpture phase, (c) unwrapped phase, (d) plane source phase, (e) depth phase, (f) the 3D outputs using plot3 command in Matlab, (g), (h) and (i) the 3D output using the *mesh* command

Then, we repeated the same procedure (using an extra fringe pattern with wavelength of 10) with the second object, human skull. The result is shown in Fig. 27.

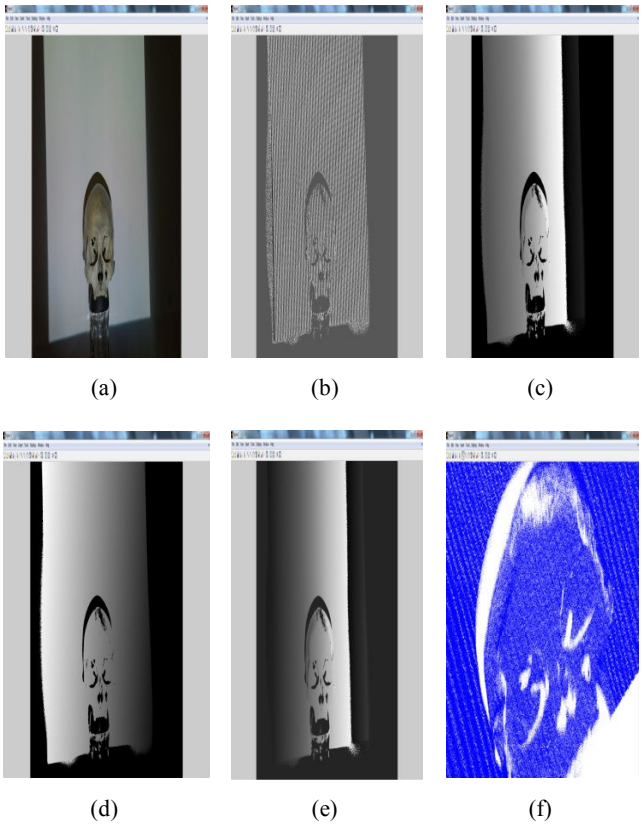

(a) (b) (c)

(d) (e) (f)

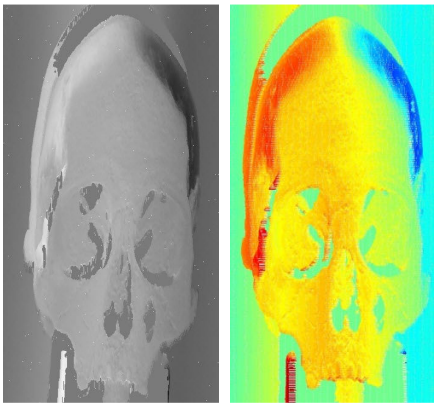

(g) (h)

Fig. 107 Using fringe pattern with wavelength of 10, (a) the original image without the fringe patterns, (b) the skull phase, (c) unwrapped phase, (d) plane source phase, (e) depth phase, (f) the 3D output using plot3 command in Matlab, (g) and (h) 3D model using mesh command

The previous experiments showed that the level of precision increases by employing more fringe patterns with shorter wavelengths.

In an attempt to reduce the computations, we repeated the same experiments with the same two objects, described previously. However, only three images (instead of six) were used to construct the 3D model. Fig. 28 and Fig. 29 show the 3D models constructed for the two objects. While, the computational times were significantly reduced, the reconstructed models are less precise, compared to the ones constructed during the previous experiments. However, it remains an attractive solution when using small/mobile devices with limited processing powers, or in some applications that do not require high accuracy.

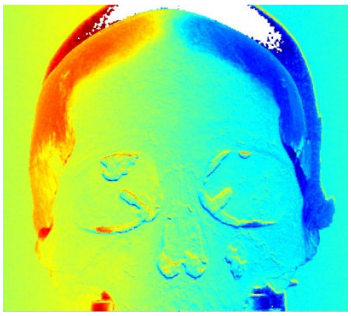

Fig. 11 3D output using three images

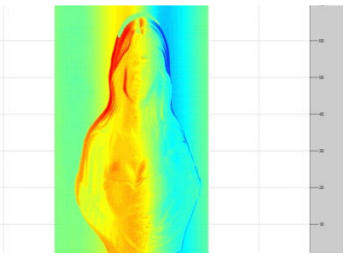

Fig. 12 3D output using three images

V. Conclusion

Fringe projection is a powerful approach for 3D reconstruction of objects. In this paper, using phase shift method for fringe pattern analysis was experimentally investigated. Fringe patterns with different wavelengths were investigated. The experiments used two objects with different attributes (e.g. size, material, level of details). Experimental results demonstrated that using patterns with shorter wavelengths captures more object details at the expense of more computational time during the phase unwrapping stage. In future, we plan to extend our experiments to consider other fringe pattern analysis approaches. We aim at using sets of objects with various features to study the response of each approach to specific object features.

References

[1] Rowe SH, Welford WT. "Surface Topography Of Non-Optical Surfaces By Projected Interference Fringe," Nature (London), 1967.
[2] S.S. Gorthi, P. Rastogi, "Fringe Projection Techniques: Whither We Are? ", Optics And Lasers In Engineering,2010,48(2)133-140.
[3] J.-F. Lin, X-Y. Su, "Two-Dimensional Fourier Transform Profilometry For The Automatic Measurement Of Three-Dimensional Object Shapes", Opt. Eng, 1995, 34 (11) 3297–3302.
[4] X. Su, W. Chen, "Fourier Transform Profilometry: A Review", Opt. Laser Eng, 2001, 35 (5)263–284.
[5] F. Berryman, P. Pynsent, J. Cubillo, "The Effect Of Windowing In Fourier Transform Profilometry Applied To Noisy Images," Opt. Laser Eng, 2001, 41 (6) 815–825.
[6] M. A. Gdeisat, D. R. Burton, M. J. Lalor, "Eliminating The Zero Spectrum In Fourier Transform Profilometry Using A Two-Dimensional Continuous Wavelet Transform", Opt. Commun, 2006, 266 (2) 482–489.
[7] P. J. Tavares, M. A. Vaz, "Orthogonal Projection Technique For Resolution Enhancement Of The Fourier Transform Fringe Analysis Method," Opt. Commun, 2006, 266 (2) 465–468.
[8] S. Li, X. Su, W. Chen, L. Xiang, "Eliminating The Zero Spectrum In Fourier Transform Profilometry Using Empirical Mode Decomposition," J. Opt. Soc. Am,2009, A 26 (5) 1195–1201.
[9] M. Dai, Y. Wang, "Fringe Extrapolation Technique Based On Fourier Transform For Interferogram Analysis With The Definition," Opt. Lett, 2009, 34 (7) 956–958.
[10] S. Vanlanduit, J. Vanherzeele, P. Guillaume, B. Cauberghe, P. Verboven, "Fourier Fringe Processing By Use Of An Interpolated Fourier-Transform Technique", Appl. Opt, 2004, 43 (27) 5206–5213.
[11] A. Dursun, S. Ozder, F. N. Ecevit, "Continuous Wavelet Transform Analysis Of Projected Fringe Patterns," Meas. Sci. Techn, 2004 15 (9) 1768–1772.
[12] J. Zhong, J. Weng, "Spatial Carrier-Fringe Pattern Analysis By Means Of Wavelet Transform: Wavelet Transform Profilometry," Appl. Opt, 2004 43 (26) 4993–4998.
[13] M. A. Gdeisat, D. R. Burton, M. J. Lalor, "Spatial Carrier Fringe Pattern Demodulation By Use Of A Two-Dimensional Continuous Wavelet Transform," Appl. Opt, 2006, 45 (34) 8722–8732.
[14] X. Su, G. Von Bally, D. Vukicevic, "Phase-Stepping Grating Profilometry: Utilization Of Intensity Modulation Analysis In Complex Objects Evaluation," Opt. Commun, 1993, 98 (1-3) 141–150.
[15] QuanC, He XY, Wang CF, Tay CJ, Shang HM. "Shape Measurement Of Small Objects Using LCD Fringe Projection With Phase Shifting," Opt Commun 2001.
[16] F. Berryman, P. Pynsent, J. Cubillo, "A Theoretical Comparison Of Three Fringe Analysis Methods For Determining The Three-Dimensional Shape Of An Object In The Presence Of Noise," Opt. Laser Eng, 2003, 39 (1) 35–50.
[17] M. A. Sutton, W. Zhao, S. R. Mcneill, H.W. Schreier, Y. J. Chao, "Development And Assessment Of A Single-Image Fringe Projection Method For Dynamic Applications, "Experimental Mechanics, 2001 41 (3) 205–217.
[18] M. A. Gdeisat, D. R. Burton, M. J. Lalor, "Eliminating The Zero Spectrum In Fourier Transform Profilometry Using A Two-Dimensional Continuous Wavelet Transform," Opt, Commun, 2006, 266 (2) 482–489.
[19] X. Su, W. "Chen, Fourier Transform Profilometry: A Review," Opt. Laser Eng, 2001 35 (5) 263–284.
[20] Y. Tangy, W. Chen, X. Su, L. Xiang, "Neural Network Applied To Reconstruction Of Complex Objects Based On Fringe Projection," Opt. Commun, 2007 278 (2) 274–278.
[21] Zhang S, Huang P. S, "High-Resolution, Real-Time Three-Dimensional Shape Measurement," Opt. Eng, 2006 45 (12) 123601.
[22] Malat S.,"A wavelet tour of signal processing," Academic Press,1999.
[23] Abid A. Z. A, "Fringe Pattern Analysis Using Wavelet Transforms," Phd Thesis, Liverpool John Moores University, 2008.
[24] Takeda M., Ina H., Kobayashi S. "Fourier–Transform Of Fringe Pattern Analysis For Computer-Based Topography And Interferometry," Journal Of Optical Society Of America,1982, Vol.72, No 1, Pp. 156-160.
[25] Bone D.J., Bachor H.A., Sandeman R.J., "Fringe-Pattern Analysis Using A 2-D Fourier Transform," Applied Optics,1986, Vol.25, No.10, 15 May.
[26] Burton D.R, Lalor M.J. "Multichannel Fourier Fringe Analysis As An Aid To Automatic Phase Unwrapping," Applied Optics,1994, 33(14):2939-48.
[27] Skydan O.A., Lalor M.J. And Burton D.R., "Technique For Phase Measurement And Surface Reconstruction By Use Of Colored Structured Light," Applied Optics,2001.
[28] Hovorov V, "A New Method For The Measurement Of Large Objects Using A Moving Sensor, "Phd Thesis, Liverpool John Moores University, 2008.